PROCEEDINGS, 41st Workshop on Geothermal Reservoir Engineering
Stanford University, Stanford, California, February 22-24, 2016
SGP-TR-209

Fractional Dynamics in Fault Structures

Anna Suzuki[1], Toshiyuki Hashida[2], Kewen Li[1] and Roland N. Horne[1]

[1] 367 Panama St, Stanford, CA 94305, USA

[2] 7-7-11-707 Aramaki-Aza-Aoba, Aoba-ku, Sendai, Miyagi 980-8579, JAPAN

anna3@stanford.edu

Keywords: tracer test, column experiment, fault zone, non-Fickian diffusion, truncated distribution, tempered anomalous diffusion

ABSTRACT

Fault zones clearly affect the flow paths of fluids at the scale of geothermal reservoirs. Fault-related fracture damage decreases to background levels with increasing distance from the fault core according to a power law. This study investigates mass transport in such a fault-related structure using nonlocal models. A column flow experiment has been conducted to create a permeability distribution that varies with distance from a main conduit. The tracer response curve describes a preasymptotic curve implying subdiffusive transport, which is slower than the normal Fickian diffusion. As long as permeability of the surrounding layers varies with distance from a main conduit, the tracer response can be modeled by the time fractional advection dispersion equation (time fADE). In contrast, if the surrounding area is a finite domain, an upper truncated behavior in tracer response (i.e., exponential decline at late time) is observed. The tempered anomalous diffusion (TAD) model captures the transition from sub-diffusive to Fickian transport, which is characterized by a smooth transition from power-law to an exponential decline in the late-time breakthrough curves.

1. INTRODUCTION

A crucial problem in geothermal reservoir engineering is to build models for fluid and heat flow systems based on incomplete information. Because of limited sampling, any model to describe regional heterogeneity necessarily will have large uncertainty. Before incorporating data from a variety of sources into the reservoir model for flow simulations, simple and quick evaluations are preferred for designing effective reinjection and production wells. Tracer testing has been used to evaluate fluid flow inside a geothermal reservoir. The flow of tracer through the reservoir provides not only qualitative information (i.e., well connectivity) but also quantitative properties by analyzing mathematical models to represent mass transport.

Traditionally, the classical advection dispersion equation (ADE) has been applied to model tracer transport in reservoirs. However, several field scale and laboratory scale tracer tests in fractured media reported significant deviations between measured breakthrough curves (BTCs) and curves obtained using the classical ADE (e.g., Neretnieks et al. 1982; Becker and Shapiro 2000; Jiménez-Hornero et al. 2005; Bauget and Fourar 2008). More specifically, in these analyses, the ADE did not capture the non-Fickian (or anomalous) behavior including a long-time tailing, which is often observed in geothermal fields (Radilla et al., 2012).

Modeling non-Fickian tracer transport in fractured and porous media has received considerable attention in recent years. Such anomalous diffusion may arise from heavy tails in the distributions of particle steps or waits due to rare extreme events, and can be modeled by nonlocal equations (e.g., the Multi-Rate Mass Transfer (MRMT) model (Haggerty and Gorelick, 1995), the Continuous Time Random Walk (CTRW) framework (Berkowitz et al., 2006), and the Fractional-Derivative Model (Benson, 2000a and 2000b; Huang et al., 2006; Zhang et al., 2009). All these approaches imply that the subsurface transport for a solute may not stay at one single diffusive state (i.e., following the same scaling rule) all the time, but rather could transfer between states of superdiffusion, subdiffusion and normal diffusion. The time fADE has been demonstrated by Schumer et al. (2003) to accurately model the time nonlocal properties of solute transport. The terminology "time nonlocal" means that the current concentration change is affected by the history of solute loading at the same location by diffusion into and out of relatively immobile zones (Zhang et al., 2009). In order to describe subdiffusion in a fractured reservoir, Fomin et al. (2011) introduces a fractal diffusion coefficient, which decays in diffusivity with distance according to a power law, into a diffusion equation.

Faults and fractures affect the flow paths at the scale of geothermal reservoirs. According to field observations in geothermal reservoirs, the main permeable zones are composed of fault-related structures, which result from a complex set of components, such as a fault core and a damage zone (Caine et al., 1996). Many quantitative studies on fault zones have shown that fault-related fracture damage decreases to background levels with increasing distance from the fault core (Anders and Wiltschko, 1994; Evans, 1988; Mitchell and Faulkner, 2009; Scholz et al., 1993; Wilson et al., 2003). Savage and Brodsky (2011) suggest that the fracture density at a damage zone decays with distance from the fault core according to a power law. Suzuki et al. (2015) conducted numerical simulations and suggests that the time fADE is a suitable model to describe a long tail of concentration in such a fault-related structure.

In contrast, field observations suggest that such a scaling between damage zone width and fault size is accurate up to a certain threshold fault size, beyond which the width of damage zone saturates (Mitchell and Faulkner, 2009; Savage and Brodsky, 2011). Meerschaert et al. (2008) proposed the tempered anomalous diffusion (TAD) model that incorporates both the classical ADE and the time fADE. They found and quantified the transition from subdiffusion to normal diffusion by using the TAD.

In this study, we investigated subdiffusion processes in a fault-related structure. Flow experiments were conducted by using a column filled with glass beads. Nonlocal modeling approaches (i.e., the time fADE and the TAD) are briefly reviewed in Section 2. Experimental procedures are shown in Section 3. Applications of the nonlocal models are discussed by using the experimental results as well as the numerical simulation results in Section 4. Conclusions are provided in Section 5.

2. THEORY

2.1 Fracture density at a fault zone

Many quantitative studies on fault zones have shown that fracture density at damage zones decreases to background levels with increasing distance from the fault core (Anders and Wiltschko, 1994; Evans, 1988; Mitchell and Faulkner, 2009; Scholz et al., 1993; Wilson et al., 2003). Savage and Brodsky (2011) suggested that the fracture density at a damage zone decays according to a power law. Suzuki et al. (2015) evaluated whether the power-law model of fracture density is applicable to fault zone architectures in a geothermal reservoir. In the work by Brogi (2008), the structural architectures of normal faults were investigated in the Rapolano geothermal area, Italy. The frequency distributions of fracture density decreased with the distance and could be fitted by power-law approximations. The power-law approximation of fracture density is valid to characterize the fracture distribution in the fault-related structure of a geothermal reservoir.

2.1 Classical advection dispersion equation (ADE)

Conventionally, the advection dispersion equation (ADE) has been used to describe mass transport underground, which can be written as (Bear, 1972):

$$\frac{\partial C}{\partial t} = \frac{D}{R_d}\frac{\partial^2 C}{\partial x^2} - \frac{u}{R_d}\frac{\partial C}{\partial x} - \xi C \tag{1}$$

The analytical solution of the ADE is:

$$C_\delta(x,t) = \frac{\Delta M}{2R_d\sqrt{\pi Dt/R_d}} \exp\left(-\frac{(x-ut/R_d)^2}{4Dt/R_d}\right) \exp(-\xi t) \tag{2}$$

where t is time. x is the distance from the injection zone. C is the concentration of tracer in the main conduit. D is the dispersion coefficient, R_d is the retardation parameter, u is the velocity, ξ describes the decay late, respectively. ΔM is the amount of injected concentration. Introducing the Peclet number ($Pe = vl/D$) and nondimensional time τ ($= t / t^*$) and distance X ($= x / l$), where t^* and l are representative variables, the normalized equation can be written as

$$R_d\frac{\partial C}{\partial \tau} = \frac{1}{Pe}\frac{\partial^2 C}{\partial X^2} - \frac{\partial C}{\partial X} - \xi' C \tag{3}$$

where $\xi' = t^* \xi R_d$.

2.2 Time fADE

Nonlocal models have been investigated to describe anomalous diffusion processes, reviewed by e.g., Neuman and Tartakovsky (2009) and Zhang et al., (2009). A fractional ADE (fADE) includes fractional derivatives on time and/or space terms (Benson et al., 2000; Schumer et al., 2003a). Traditional mobile-immobile models (i.e., dual porosity/permeability models) assume that particles move between the mobile and immobile phases at an instantaneous rate proportional to the difference in concentration. In contrast, the time fADE uses a memory function to govern release from the immobile phase (Haggerty, 1995), which has been used to fit late-time solute breakthrough curves in groundwater aquifers (Haggerty, 2000).

The time-fractional advection dispersion model (time fADE) can be written as (Schumer et al., 2003; Fomin et al., 2011):

$$\frac{\partial C}{\partial \tau} + b\frac{\partial^\gamma C}{\partial \tau^\gamma} = \frac{1}{Pe}\frac{\partial^2 C}{\partial X^2} - \frac{\partial C}{\partial X} \tag{4}$$

where b is the retardation coefficient related to diffusion processes in the surrounding rocks, and $b\frac{\partial^\gamma C}{\partial \tau^\gamma}$ is the Caputo fractional derivative with respect to time of order γ ($0 < \gamma \leq 1$) defined in Samko (1993).

The second term of the left-hand side in the time fADE (4) models the solute diffusion process in a fault-related structure. This term comes from the mass flux into the surrounding rock as follows:

$$
\begin{aligned}
J_f &= -D_0 Y^{-\theta} \frac{\partial C}{\partial Y}\bigg|_{Y=0} \\
&= -\int_0^t \frac{\partial C}{\partial \zeta} D_0 Y^{-\theta} \frac{\partial C(Y, t-\zeta)}{\partial Y}\bigg|_{Y=0} d\zeta \\
&= \int_0^t \frac{\partial C}{\partial \zeta} \Phi(t-\zeta) d\zeta
\end{aligned}
\tag{5}
$$

where D_0 is the diffusivity at the main conduit along the fault core (X-axis), and Y is the distance from the main conduit, which is perpendicular to the X direction. θ is an index describing the decay in diffusivity. Φ is a memory function which is selected based on.transport behavior. Because the memory function follows a power law, the time fractional derivative appears in the time fADE model (4) (Haggerty et al., 2000; Scher et al., 2002; Schumer et al., 2003a).

2.2 Tempered anomalous diffusion model (TAD)

After most of the solute mass is flushed out through the main conduit with high-permeability, the remaining solutes trapped in the surrounding low-permeability layers will diffuse out and produce macroscopic subdiffusive transport behavior. The thickness of surrounding layers constrains the maximum waiting time and results in an eventual transition from sub-diffusive to Fickian transport, observed as a smooth transition from power-law to exponential decline in the late-time breakthrough curves. This pre-asymptotic transport is directly linked to the exponentially truncated power-law distribution of waiting times. To capture the exponentially truncated power-law distribution of waiting times for solute particles trapped in the parallel immobile phases, Meerschaert et al. (2008) proposed the incomplete Gamma function:

$$
\Phi(t) = \int_t^{\infty} e^{-\lambda t} \frac{\gamma \tau^{-\gamma-1}}{\Gamma(1-\gamma)} d\tau
\tag{6}
$$

as memory function, where $\lambda > 0$ is the truncation parameter in time. Substituting (6) into the mass flux (5) and modifying Eq. (4), one obtains the tempered anomalous diffusion model for transient non-Fickian diffusion (Meerschaert et al., 2008):

$$
\frac{\partial C}{\partial \tau} + b e^{-\lambda t} \frac{\partial^{\gamma}}{\partial \tau^{\gamma}} (e^{\lambda t} C) - b\lambda^{\gamma} C = \frac{1}{Pe} \frac{\partial^2 C}{\partial X^2} - \frac{\partial C}{\partial X}
\tag{7}
$$

When $\gamma = 1$, the TAD (7) is correspond to the classical ADE model, Eq. (3), where $R_d = 1 + b$.

Figure 1 illustrates the feature of TAD model (7). We expect that the TAD model (7) can capture mass transport in a fault zone where fracture density shows upper truncated power-law distributions.

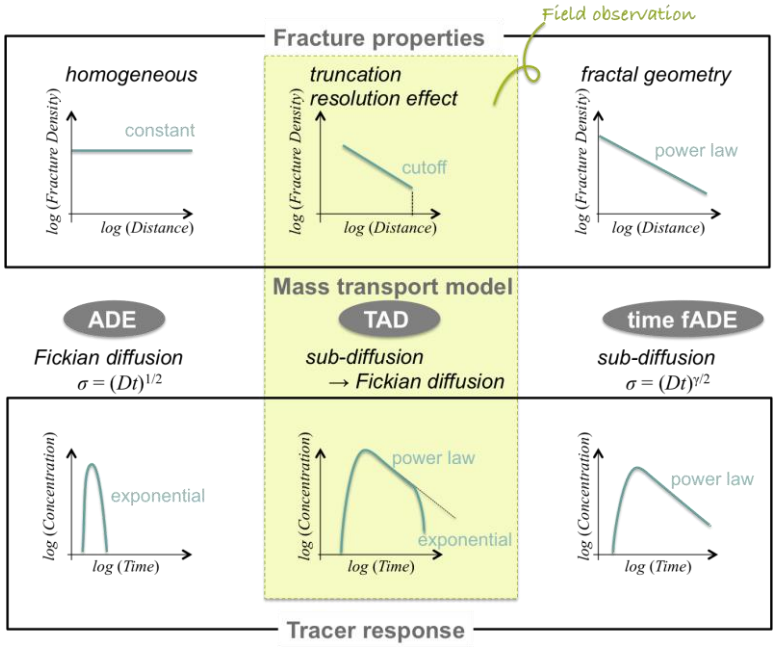

Figure 1: Feature of the TAD model in terms of fracture properties and tracer response behavior.

3. COLUMN EXPERIMENTS

3.1 Experimental methods

Tracer flow experiments were designed using flow columns filled with glass beads to evaluate the effect of permeability distribution. Figure 2 illustrates the operation of the column apparatus. A 10-inch long, 3.8-inch internal diameter glass column was packed with glass beads. Different diameters of glass beads provided a spatial distribution of permeability for the fault zone model.

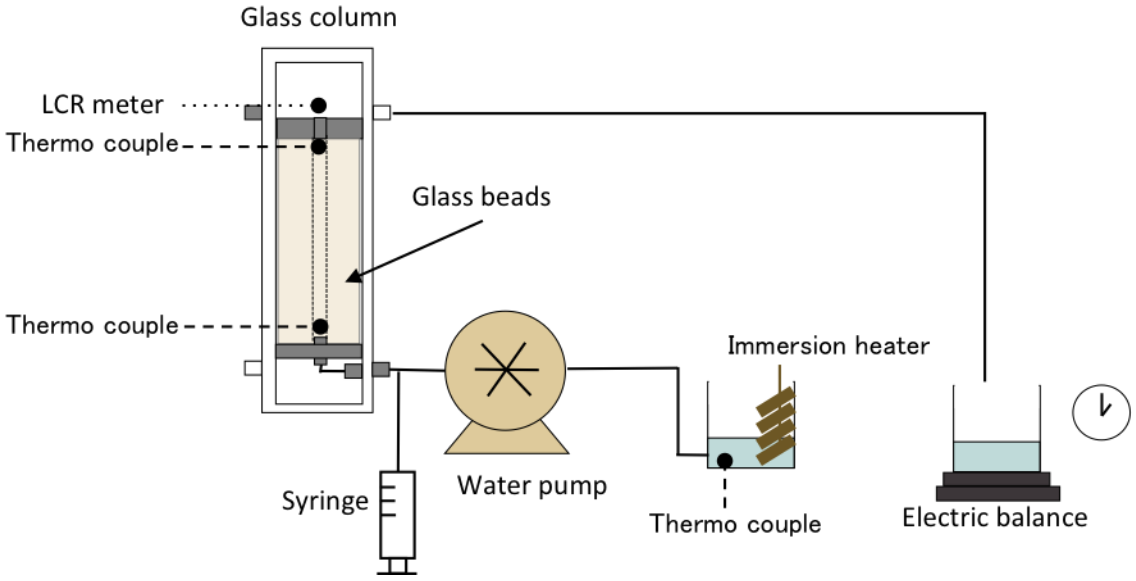

Figure 2: Schematic of experimental apparatus.

The inside of the column was divided into four areas (I, II, III, and IV) each with different size of glass beads. First, thin-walled tubings were used to separate the column into the four "layers" (rings). The inner diameters of the tubings were 0.25 in., 0.5 in. and 1 in., respectively. The largest glass beads were set in the innermost layer (I), while the smallest ones were allocated in the outermost layer (II). The thin wall tubing was packed with glass beads in 1-cm increments by pouring freshwater into the tube and pressing the beads down, and eventually withdrawn.

For comparison, a single-layer model was also employed to evaluate the effect of permeability distribution. The single-layer model consists of only the innermost layer (I). The tubing with inner diameter of 0.25 in. remained in the column. The setting of glass beads and saturation for the single-layer model followed the same procedure as the fault zone model.

Prior to the tracer flow test, the permeability of the glass beads of different sizes was measured in a bead-filled cylinder with radius of 3.69 cm. The total amount of water flowing through the system was determined by measuring the weight of water in the exit container using a balance (Mettler balance, Model PE 300) over time. The accuracy of the balance is 0.01g.

The water head difference between the inlet and the outlet was held constant for each permeability measurement, and the flow rate was measured three times (or more) for each head difference. Measurements from three head differences in the range between 17 cm and 22 cm were used to calculate the average permeability for each glass bead size. Darcy's law for horizontal flow was utilized to compute the permeability given as:

$$K = \mu QL / \rho gAht \tag{8}$$

where Q is the volume of water [m^3], A is the surface of cylinder [m^2], t is time [s], h is the water head difference [m], L is the length of the flow path (layer of glass beads) in the cylinder [m]. We used μ = 0.000102 [kg s m^{-2}] for the viscosity and ρ = 1.0 [kg m^{-3}] for the density water at room temperature (25 °C).

Measured permeability values were compared to theoretical values of permeability for various glass bead sizes as calculated by (Lappen et al., 1997):

$$K = \frac{D^2\epsilon^3}{150(1-\epsilon)^2}, \tag{9}$$

where K is the permeability [m^2], D is the diameter of glass beads [m], and ε is the porosity. This study used glass beads with diameters of 0.500-0.707 mm (Area I), 0.354-0.500 mm (Area II), 0.177-0.297 mm (Area III), and 0.044-0.088 mm (Area IV). This allocation can generate an approximate permeability distribution associated with the value of θ = 2.

For the tracer experiment, the column was saturated from below with pure water at 25 °C. Water was injected through an injection loop using the water pump (Dynamax) from the bottom of the column. The injection rate and temperature were kept constant at 0.7 cm^3/ min and 25 °C, respectively. In this study we focused on the effect of permeability distribution on tracer response curves, so the thermal effect was neglected. The column was flushed with pure water prior to the tracer injection. The flow rate was measured over time using the balance at the outlet in the same manner as the permeability measurement.

Sodium chloride (NaCl) tracer was added to the inflow to the column as an impulse change in concentration. The experiments used a NaCl concentration of 2.5 % by weight. Concentrations of the tracer NaCl during the experiment were determined by measuring the electrical resistance of the fluid exiting the column, using a LCR meter (DE-6000-LCR, iET Labs, Inc.) at a frequency of 1 kHz.

3.2 Experimental results

For each tracer experiment, measurements were recorded throughout the entire evolution of the tracer plume. The series resistance of water was measured at the column outlet to estimate electrical conductivity. NaCl concentration was then determined from the electrical conductivity of the solution. In our experiments, the electrical conductivity showed a power-law relation with NaCl concentration in the range from 0.01 % to 2.5 %, which was consistent with the trend in CRC Handbook of Chemistry and Physics. Concentrations were normalized by setting the background concentration to C = 0 and the injected tracer concentration of 2.5% to C = 1. Breakthrough curves were plotted as normalized concentration versus time. Measurement error in the curve includes the sensitivity of the resistance measurement.

A concentration profile for the single-layer model is displayed in Figs. 3(a) and (b) in linear and log-log plots, respectively. The tracer curve for the single-layer model shows a sharp peak at an early time but no tail at late time. The result indicates that the tracers migrate as a single cluster and advection is dominant. In contrast, Figs. 3(c) and (d) plots tracer responses for the fault-zone model using different sizes of glass beads. The peak concentration for the fault zone model is lower than that for the single-layer model. At late times, a gradual decrease in tracer concentration was observed.

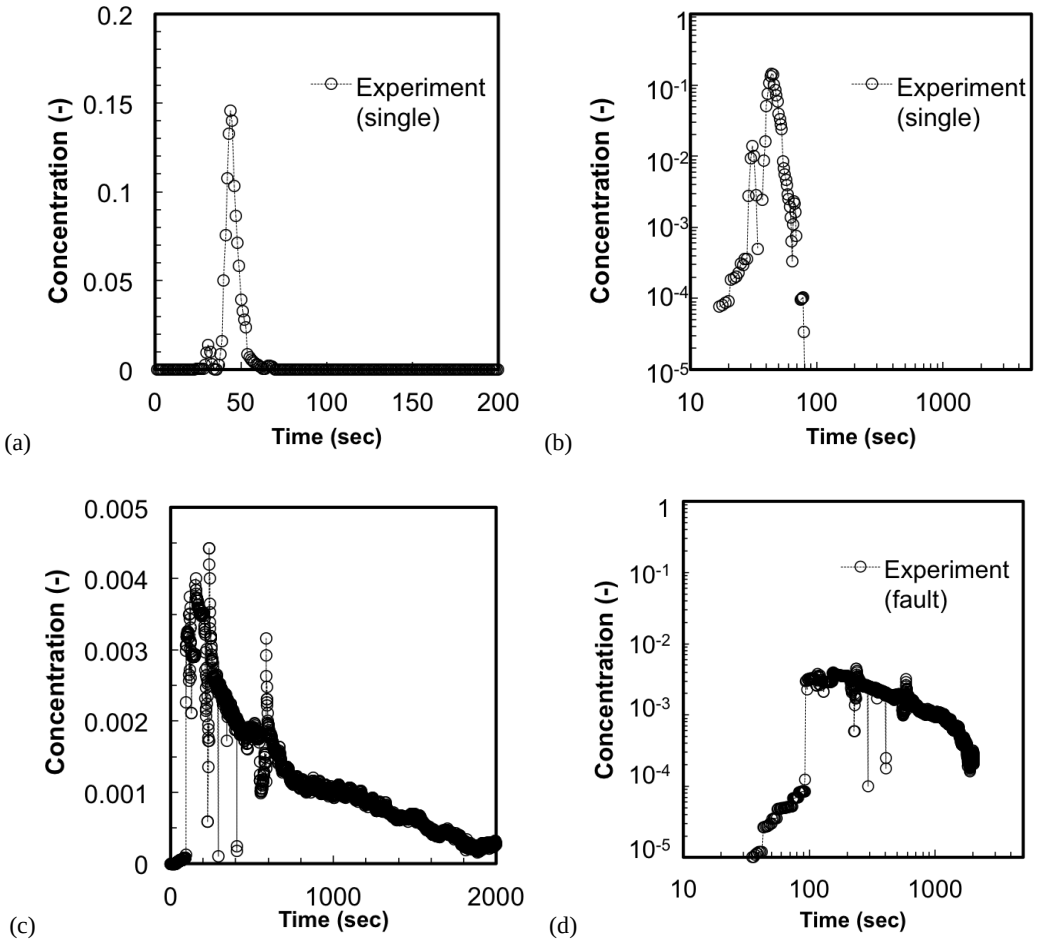

Figure 3: Tracer breakthrough curves in column experiment: (a) linear plot and (b) semi-log plot for the single-layer model and (c) linear plot and (d) semi-log plot for the fault zone model.

Figure 4 shows flow-storage diagrams obtained from tracer responses for the single layer and the fault zone models, respectively. The tracer responses can be used semiquantitatively to describe reservoir geometry. When the flow and storage capacities are uniform in each conduit, the flow-storage curve is a straight line. The flow storage diagram shows approximately straight line for the single-layer

model (Fig. 4(a)). Fig. 4(b) describes the flow storage diagram for the fault zone model. We observed an arc curve, which means that 50% of the flow comes from 25% of the pore volume. This finding indicates that there are preferential flow paths in the fault zone model.

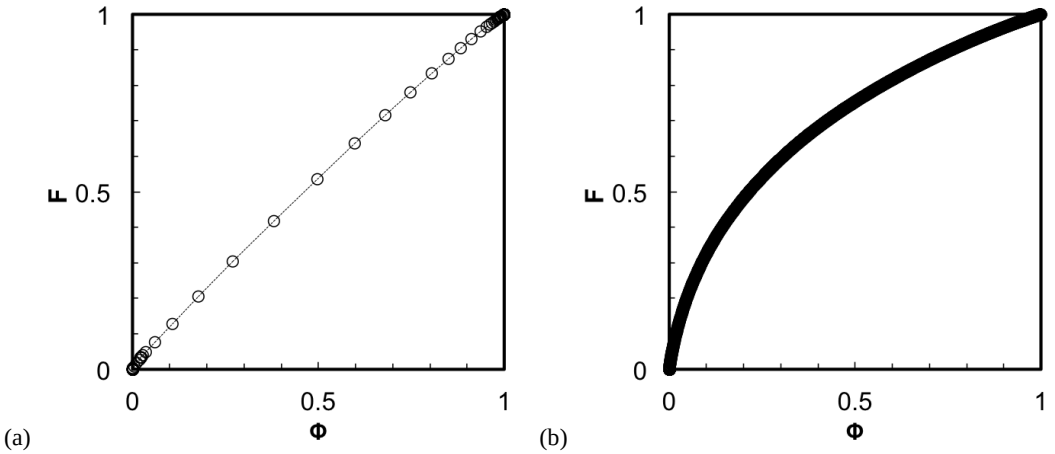

Figure 4: Flow storage diagrams (a) for the single-layer model and (b) for the fault zone model.

4. APPLICATIONS

4.1 Simulation results

Suzuki et al. (2015) conducted synthetic numerical simulation by using TOUGH2 (Pruess, 2011) to reveal influences of the structure in a fault zone and to verify the applicability of the time fADE model (5). The reservoir was assumed to be homogeneous and to consist of a main conduit and the surrounding rocks. The main conduit is along a fault core with high permeability, while the surrounding rocks has a fracture density that decays with distance from the fault core. The simulations assume that the surrounding rock is in the semi-infinite domain and the fracture density distribution is described as a permeability distribution.

Figures 5 show the tracer response simulated by TOUGH2. The tracer response for the single-layer model displays a symmetric curve because the tracer transport was governed solely by advection. This curve is consistent with the experimental results presented in previous Session 3. On the other hand, tracer responses for the fault zone model produced a linear decrease in the concentration on a log–log scale. This indicates that the tail can be approximated by a power law. Suzuki et al. (2015) also presented the results for the two-layer model, in which the permeability of surrounding rocks are constant and lower than the permeability in the main conduit. The two-layer model produced two distinct peaks in the tracer response corresponding to the two clusters of tracers. Some tracer appearing in the first peak travels only in the main conduit, while the others migrate into the surrounding rocks and eventually are released back into the main fluid. As long as the tracer migrates into the lower permeable zone more than once, the tracer retards from the fastest cluster. In comparison with the two-layer model, the fault zone model changes in permeability continuously and causes gradual decay in concentration in the tracer response curve. The gradual decline of concentration indicates a retardation of tracer migration into the surrounding rocks that cannot be distinguished as countable clusters. The gradual decrease in the concentration corresponding to a power law, as shown in Fig. 5(b), is a feature of tracer response curve with the fault zone model.

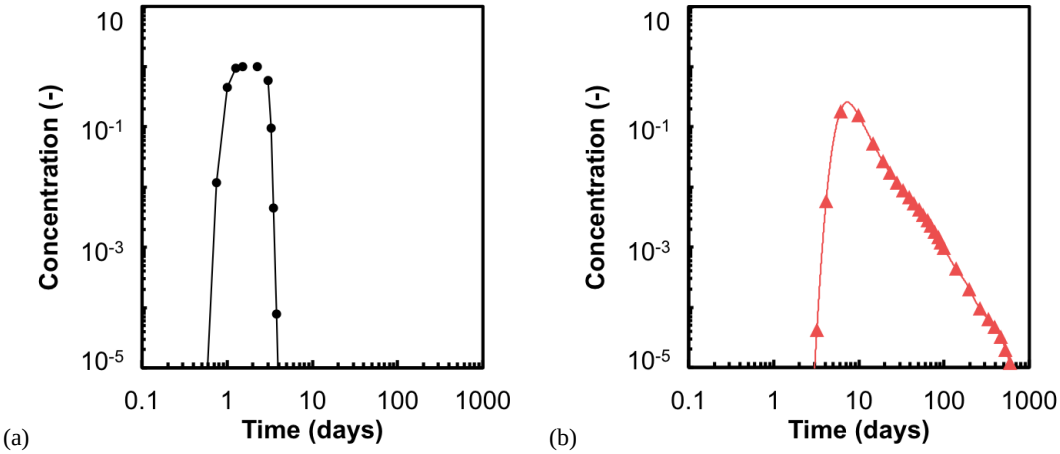

Figure 5: Effects of different permeability distributions on tracer responses calculated by TOUGH2: (a) single-layer and (b) fault zone models.

4.2 Solution of time fADE

Figure 6 shows example solutions of the time fADE (4). The time-fractional parameter γ codes retention and can be estimated from the late-time tail of the breakthrough curve (Schumer et al., 2003). The waiting time density is a heavy-tailed distribution that reflects the presence of long rest periods for tracers in storage. A suitable description of the tracer behavior may be obtained from a time fADE model with a fractional time term (Schumer et al., 2009). The standard deviation of the solution can be written as $\sigma = (Dt)^{\gamma/2}$. Because σ grows at a rate slower than ‘‘normal’’ Fickian dispersion when $0 < \gamma < 1$, this behavior is referred to as subdiffusive. This characterizes a ‘‘long memory’’ effect, in which current tracer flow is influenced by events far back in time. As shown in Fig. 5, the solution of the classical ADE (3) shows a symmetric curve, while the solutions by the time fADE (4) with γ =0.1, 0.5 appear to decay at late times with a power law. When subdiffusion occurs due to spatial variation of diffusivity, the time fADE is a preferred model for characterization of mass transport in the fault-related structures. As shown in Fig. 5(b), the tail in the simulated tracer response for the fault zone model presented an approximate straight line on a log–log plot. This observation provides strong evidence that the time fADE can be used to simulate mass transport in structures where diffusion decreases with distance according to a power law.

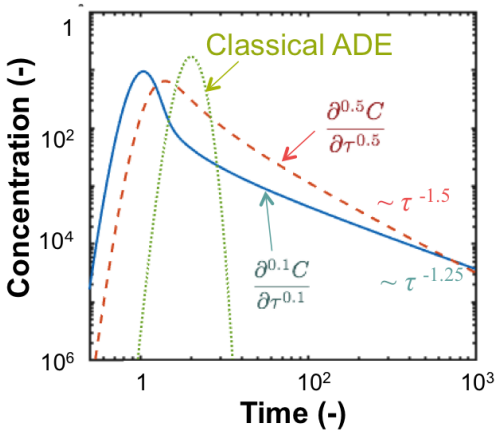

Figure 6: Solutions of the time fADE.

Figure 7 shows the experimental results of tracer response for the fault zone model. The experimental data in the time interval between 0.6 and 6 matches a trend to decrease in concentration with a power law over time, while the data after time 6.0 shows a significant difference from the power law approximation. The upper truncated power-law distributions can be found in many geophysical processes at various scales including long-term retention of contaminants in alluvial aquifers (Zhang et al., 2009). The TAD model describes such upper truncation behaviors by using a cutoff parameter λ to apply power law models to practical problems in geophysics. Zhang and Lv (2007) comment that natural heterogeneous media may exhibit a much longer persistence of anomalous diffusion and the exponential tempering parameter λ is related to retention time in immobile zones. Zhang et al. (2007) argue that the thickest immobile materials with the slowest decay rates control the transition of the late-time breakthrough curve from power-law to exponential, implying that λ relates to the retention time in the immobile blocks. In our experiment, we use a column with finite diameter. The length of the surrounding area in the column (layer II, III, and IV) is a threshold of this system and caused the upper truncation behavior in the tracer response. In fault zones, the damage zone width, i.e. the distance at which the fault-related damage drops to background levels, has been recognized as the threshold of the damage zone (Mitchell and Faulkner, 2009; Savage and Brodsky, 2011). Thus, the λ might correlate to the width of the damage zone. The quantitative relationship between the exponential tempering parameter λ and the damage zone width will be explored in further studies.

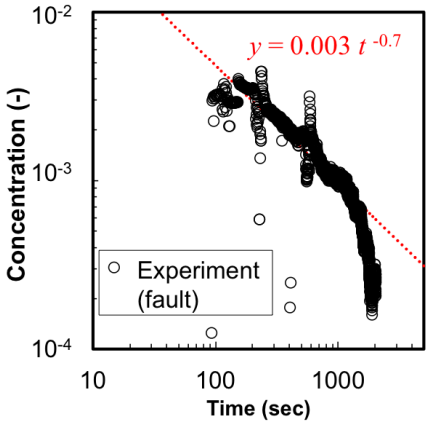

Figure 6: Experimental result for the fault zone model and power law approximation.

4.3 Experimental results

The tracer concentration and time obtained from the column experiment are normalized by injected concentration and peak time, respectively. To compare the models, the root-mean-square error (RMSE) is used to assess the goodness of fit.

We first fit the breakthrough curve for the single-layer model by using analytical solution of the classical ADE (1). We neglected the retardation parameter R_d and the decay rate ξ in order to consider the simplest scenario, and estimated v and D in the ADE model (1) by using the Gauss-Newton method to minimize the RMSE. The best-fit v and D were 1 and 0.005, respectively. The fitted ADE solution matched the data well, as shown by the solid lines in Fig. 8. The result is consistent with the simulation result discussed in the previous session. Thus, that mass transport for the single-layer model in this experimental system can be adequately described by the classical ADE model (1).

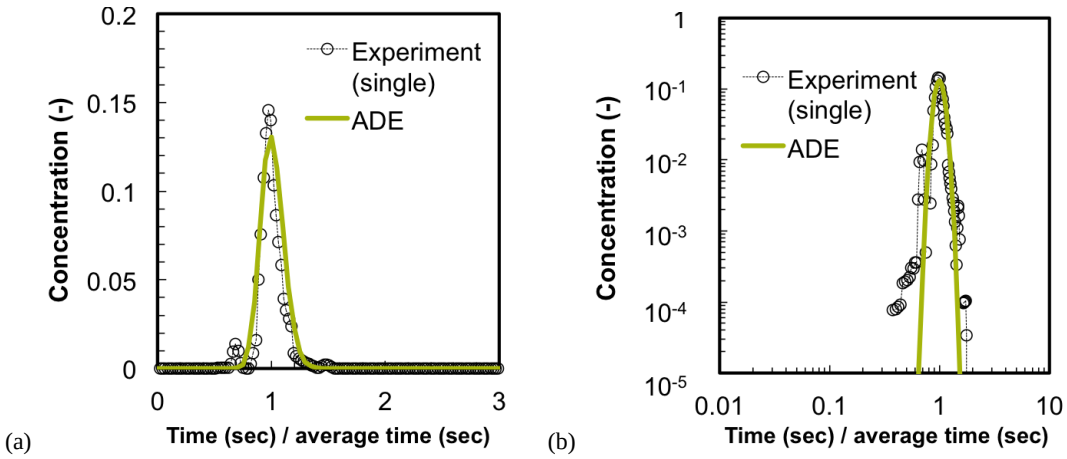

Figure 8: Fitted curve by the classical ADE (line) to experimental tracer response curve (circles): (a) linear scale and (b) log-log scale.

Next, the breakthrough curve for the fault zone model is fitted by the classical ADE model (1) including R_d and ξ. When using all data to estimate parameters (ADE #1), the parameters were determined to v = 0.01, D = 0.57, R_d = 13.1, and ξ = 0.003, respectively. Effective velocity calculated by the peak time and the length between the inlet and the outlet is 0.0015 m/s. The estimated velocity was one order larger than the effective velocity. The solid line in Fig. 8 describes the best-fit curve (ADE #1), which overestimates the early-time behavior and underestimates the peak in the breakthrough curve (Fig. 9). Overall, the ADE #1 is reasonably able to capture the tracer flow behavior including long-time. As mentioned previously, we used a column with finite diameter in this experiment, which generated the upper truncated behavior in the breakthrough curve. If the width of the surrounding areas does not produce anomalous diffusion compared to the migration distance of tracer (i.e., a distance between an inlet and an outlet), the system follows the same scaling rule and the ADE model captures the general behavior of the tracer response at a macroscopic scale.

In order to capture the peak concentration, data up to time 2.0 s was used to estimate parameters for the second model (ADE #2). The best-fit parameters were $v = 1 \times 10^{-7}$, D = 0.005, R_d = 0.42, ξ = 1.77, respectively. The dashed line in Fig. 8 plots the best-fit curve (ADE #2). Although the ADE #2 can capture the peak in the breakthrough curve, the late-time behavior was overestimated (Fig. 9). The estimated velocity was extremely smaller than the effective velocity. The best-fit parameters were unsuitable to describe transport in this system.

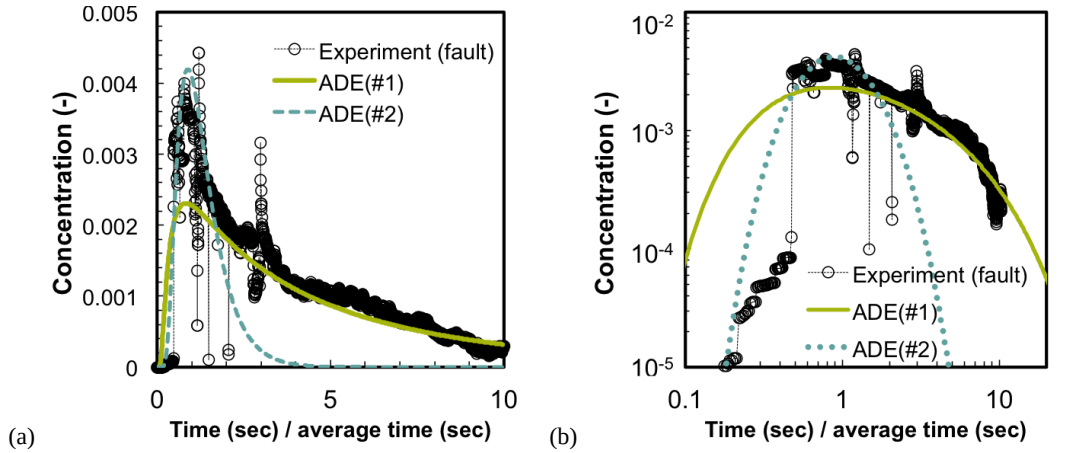

Figure 9: Fitted curve by the classical ADE (lines) to experimental tracer response curve (circles): (a) linear scale and (b) log-log scale.

As discussed in Section 2, the Tempered anomalous diffusion (TAD) model (7) is able to describe upper truncated behavior, as observed in the tracer response for the fault zone model in this experiment. Thus, we applied the TAD model (7) to the experimental result for the fault zone model. An implicit finite difference method yields the numerical solution of the TAD model (7), which can be found in Zhang et al. (2014). The breakthrough curve for the fault zone model is captured by the TAD model (7) as shown in Fig. 9. The TAD model (7) was in reasonable agreement with the peak of the tracer response and long tail at late times, compared with the fitted result by ADE #1 shown in Fig. 8. The best-fit parameters are b =2.0, Pe =8.0, γ = 0.3, and λ = 0.05. The equation is normalized and describes the ratio of advection to dispersion as Peclet number. When Pe > 1, advection is dominant in the system. We assumed there is a one-dimensional main conduit (innermost layer I) where advection is dominant and that tracer subsequently diffuses into the surrounding area. Therefore, our estimated value of Pe = 8 is reasonable. In contrast, the Peclet numbers for the ADE #1 and ADE #2 ($Pe = vl / D$) are 5.4×10^{-3} and 3.0×10^{-8}, respectively. These numbers implies that the traditional ADE model (1) describes the two-dimensional diffusion as one dispersion coefficient, which is insufficient for the fault zone behavior.

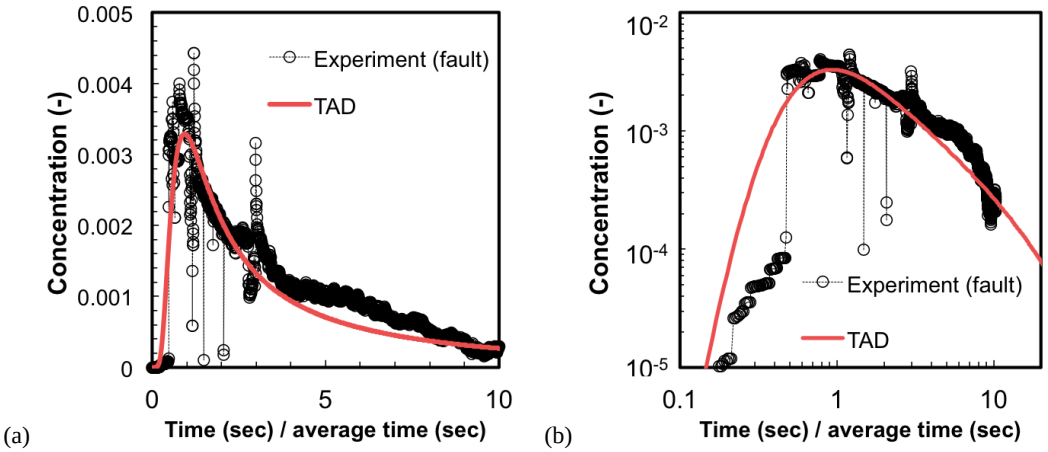

Figure 10: Fitted curve by the tempered anomalous diffusion (TAD) model (lines) to experimental tracer response curve (circles): (a) linear scale and (b) log-log scale.

Figure 11 shows the solution of the TAD model (7) with different λ. The other parameters such as b, γ, and Pe are the same as obtained by the curve fitting above. According to Haggerty et al. (2000), the tracer concentration at a late time can be approximated by the memory function. At time $t << 1 / \lambda$, the power-law exponent dominates, leading to a power-law decline of tracer concentration. In contrast, when the time is large $t >> 1 / \lambda$, the TAD model is dominated by the exponential term, leading to a fast decline of tracer mass. Zhang et al. (2014) suggests that the power-law slope is $-\gamma$ if the truncation parameter λ is small (the dotted line in Fig. 10). Our findings are consistent with the standard time fADE (4) (with λ= 0) because the TAD model (7) reduces to the standard time fADE model (4) if $\lambda \rightarrow 0$. Conversely, when $\lambda \rightarrow 1$, there is no power-law tail for arrival times larger than $1 / \lambda$ (the dashed line in Fig. 10). Therefore, the truncation parameter λ captures the transition from power-law to exponential decline for the breakthrough curve at late times. In our experiment, the tracers first distributes as a power law for the outside layers (II, III, and IV), and then they migrate as exponential due to the finite diameter of the column.

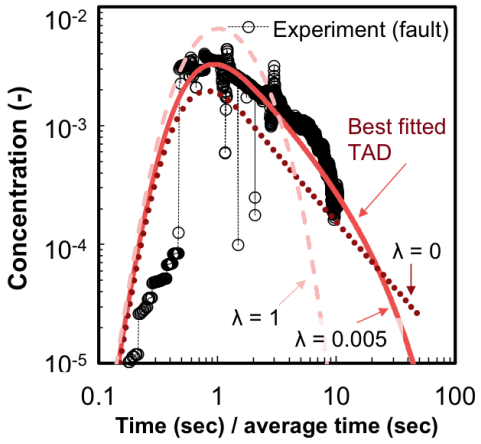

Figure 11: Effect of the truncation parameter λ.

In real fields, many quantitative studies on fault zones have shown that both fault-related fracture damage decreases to background levels with increasing distance from the fault core (Anders and Wiltschko, 1994; Evans, 1988; Mitchell and Faulkner, 2009; Scholz et al., 1993; Wilson et al., 2003). The damage zone width, i.e. the distance at which the fault related damage drops to background levels

has been recognized as the threshold of the damage zone (Mitchell and Faulkner, 2009; Savage and Brodsky, 2011). Thus, for a suitable model to describe truncated behaviors at fault zones, it is important to take this threshold into account. As shown in Fig. 1, the TAD model is expected to model mass transport in a fault zone where the fracture density shows the upper power law distribution. Experimental results are strong evidences of the applicability of the TAD model. The TAD model including the truncation parameter λ is expected to capture mass transport at a damage zone and to bridge between the conventional local models (i.e., the classical ADE model) and the nonlocal models (i.e., time fADE model).

5. CONCLUSIONS

Numerical simulations and column flow tests were conducted to generate tracer responses in a single-layer and in a fault-related structure. Both numerical and experimental tracer responses for the single-layer model show a symmetric sharp peak at early time, which can be described by the classical advection dispersion equation (ADE). On the other hand, numerical results simulating tracer responses with a fault-related structure produced decrease in the concentration of tracer as a power law; this behavior corresponds to a solution of the time fractional advection dispersion equation (time fADE). Our findings provide strong evidence that the time fADE can describe mass transport into the outside layers where diffusivity decays with distance according to a power law. On the other hand, the tracer response for the fault zone model obtained from laboratory experiments showed a preasymptotic and upper truncated behavior. This response is affected by the finite diameter of the column in this experiment. The finite thickness of diffusion-limited layers results in an exponentially truncated waiting time distribution for solute particles reaching those outside layers. The tempered anomalous diffusion (TAD) model is in better agreement with the tracer response including the upper truncated behavior, and bridges between the conventional local and the nonlocal models.

ACKNOWLEDGEMENTS

This work was supported by the Japan Society for the Promotion of Science, under JSPS Postdoctoral Fellowships for Research Abroad (H26-416), whose support is gratefully acknowledged.

REFERENCES

Anders, M.H., Wiltschko, D. V., 1994. Microfracturing, paleostress and the growth of faults. J. Struct. Geol. 16, 795 – 815.

Bauget, F., Fourar, M., 2008. Non-Fickian dispersion in a single fracture. J. Contam. Hydrol. 100, 137–48. doi:10.1016/j.jconhyd.2008.06.005

Bear J. Dynamics of Fluids in Porous Media. New York: American Elsevier; 1972.

Becker, M.W., Shapiro, A.M., 2000. Tracer transport in fractured crystalline rock: Evidence of nondiffusive breakthrough tailing. Water Resour. Res. 36, 1677–1686. doi:10.1029/2000WR900080

Benson, D. a. D.A., Wheatcraft, S.W.S.W., Meerschaert, M.M., 2000. Application of a fractional advection-dispersion equation. Water Resour. Res. 36, 1403–1412. doi:10.1029/2000WR900031

Benson, D.A., Wheatcraft, S.W., Meerschaert, M.M., 2000. The fractional-order governing equation of Lévy motion. Water Resour. Res. 36, 1413–1423.

Berkowitz, B., Cortis, A., Dentz, M., Scher, H., 2006. Modeling non-fickian transport in geological formations as a continuous time random walk. Rev. Geophys. 44, 1–49. doi:10.1029/2005RG000178.1.INTRODUCTION

Brogi, A., 2008. Fault zone architecture and permeability features in siliceous sedimentary rocks: Insights from the Rapolano geothermal area (Northern Apennines, Italy). J. Struct. Geol. 30, 237–256. doi:10.1016/j.jsg.2007.10.004

Caine, J.S., Evans, J.P., Forster, C.B., 1996. Fault zone architecture and permeability structure. Geology 24, 1025–1028.

Clauset, A., Shalizi, C.R., Newman, M.E.J., 2009. Power-Law Distributions in Empirical Data. SIAM Rev. 51, 661–703.

Evans, J.P., 1988. Deformation mechanisms in granitic rocks at shallow crustal levels. J. Struct. Geol. 10, 437–443.

Fomin, S. a., Chugunov, V. a., Hashida, T., 2011. Non-Fickian mass transport in fractured porous media. Adv. Water Resour. 34, 205–214. doi:10.1016/j.advwatres.2010.11.002

Haggerty, R., Gorelick, S.M., 1995. Multiple-rate mass transfer for modeling diffusion and surface reactions in media with pore-scale heterogeneity. Water Resour. Res. 31, 2383–2400.

Haggerty, R., McKenna, S., Meigs, L.C., 2000. On the late-time behavior of tracer test breakthrough curves. Water Resour. Res. 36, 3467–3479.

Huang, G., Huang, Q., Zhan, H., 2006. Evidence of one-dimensional scale-dependent fractional advection-dispersion. J. Contam. Hydrol. 85, 53–71. doi:10.1016/j.jconhyd.2005.12.007

Jimenez-Hornero, F.J., Giraldez, J. V., Laguna, A., Pachepsky, Y., 2005. Continuous time random walks for analyzing the transport of a passive tracer in a single fissure. Water Resour. Res. 41. doi:10.1029/2004WR003852

Meerschaert, M.M., Zhang, Y., Baeumer, B., 2008. Tempered anomalous diffusion in heterogeneous systems. Geophys. Res. Lett. 35, 1–5. doi:10.1029/2008GL034899

Meerschaert, M.M., Zhang, Y., Baeumer, B., 2010. Particle tracking for fractional diffusion with two time scales. Comput. Math. with Appl. 59, 1078–1086. doi:10.1016/j.camwa.2009.05.009

Mitchell, T.M., Faulkner, D.R., 2009. The nature and origin of off-fault damage surrounding strike-slip fault zones with a wide range of displacements : A field study from the Atacama fault system , northern Chile. J. Struct. Geol. 31, 802–816. doi:10.1016/j.jsg.2009.05.002

Neretnieks, I., Eriksen, T., Tahtinen, P., 1982. Tracer movement in a single fissure in granitic rock: Some experimental resutls and their interpretation. Water Resour. Res. 18, 849–858.

Neuman, S.P., Tartakovsky, D.M., 2009. Perspective on theories of non-Fickian transport in heterogeneous media. Adv. Water Resour. 32, 670–680. doi:10.1016/j.advwatres.2008.08.005

Pruess, K., Moridis, G., 2011. TOUGH2 User's guide, Version 2 43134.

Radilla, G., Sausse, J., Sanjuan, B., Fourar, M., 2012. Interpreting tracer tests in the enhanced geothermal system (EGS) of Soultz-sous-Forêts using the equivalent stratified medium approach. Geothermics 44, 43–51. doi:10.1016/j.geothermics.2012.07.001

Samko, SG, Kilbas, AA, Marichev, OI. Fractional integrals and derivatives: theory and applications. London: Gordon and Breach; 1993.

Savage, H.M., Brodsky, E.E., 2011. Collateral damage: Evolution with displacement of fracture distribution and secondary fault strands in fault damage zones. J. Geophys. Res. 116. doi:10.1029/2010JB007665

Scher, H., Margolin, G., Metzler, R., Klafter, J., Berkowitz, B., 2002. The dynamical foundation of fractal stream chemistry : The origin of extremely long retention times. Geophys. Res. Lett. 29, 2–5.

Scholz, C.H., Dawers, N.H., Yu, J.Z., Anders, M.H., Cowie, P.A., 1993. Fault growth and fault scaling laws: Preliminary results. J. Geophys. Res. 98, 21951–21961.

Schumer, R., Benson, D. a., Meerschaert, M.M., Baeumer, B., 2003. Fractal mobile/immobile solute transport. Water Resour. Res. 39. doi:10.1029/2003WR002141

Schumer, R., Meerschaert, M.M., Baeumer, B., 2009. Fractional advection-dispersion equations for modeling transport at the Earth surface. J. Geophys. Res. Earth Surf. 114, 1–15. doi:10.1029/2008JF001246

Suzuki, A., Niibori, Y., Fomin, S., Chugunov, V., Hashida, T., 2015. Prediction of reinjection effects in fault-related subsidiary structures by using fractional derivative-based mathematical models for sustainable design of geothermal reservoirs. Geothermics 57, 196–204. doi:10.1016/j.geothermics.2015.04.001

Wilson, J.E., Chester, J.S., Chester, F.M., 2003. Microfracture analysis of fault growth and wear processes, Punchbowl Fault, San Andreas system, California. J. Struct. Geol. 25, 1855–1873. doi:10.1016/S0191-8141(03)00036-1

Zhang, X., Lv, M., 2007. Persistence of anomalous dispersion in uniform porous media demonstrated by pore-scale simulations. Water Resour. Res. 43, n/a–n/a. doi:10.1029/2006WR005557

Zhang, X., Lv, M., Crawford, J.W., Young, I.M., 2007. The impact of boundary on the fractional advection–dispersion equation for solute transport in soil: Defining the fractional dispersive flux with the Caputo derivatives. Adv. Water Resour. 30, 1205–1217. doi:10.1016/j.advwatres.2006.11.002

Zhang, Y., Benson, D.A., Reeves, D.M., 2009. Time and space nonlocalities underlying fractional-derivative models: Distinction and literature review of field applications. Adv. Water Resour. 32, 561–581. doi:10.1016/j.advwatres.2009.01.008